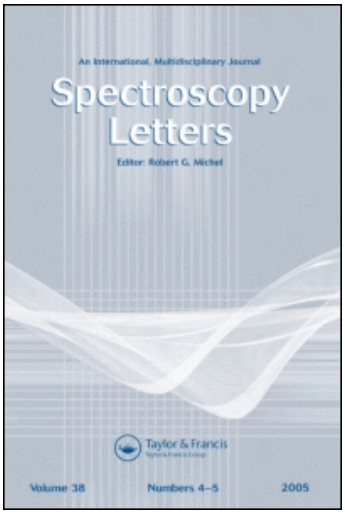

Spectroscopy Letters
Publication details, including instructions for authors and subscription information:
http://www.informaworld.com/smpp/title~content=t713597299

Studies of Atmospherically Relevant Reactions Using Differentially Pumped Mass Spectrometer and Fourier Transform Infrared Spectroscopy

Hui Yan[a]; Liang T. Chu[a]; Ronghua Jin[b]; Guowang Diao[c]
[a] Wadsworth Center, New York State Department of Health and Department of Environmental Health Sciences, School of Public Health, SUNY-Albany, Albany, New York, USA [b] Department of Chemistry, Shanghai Normal University, Shanghai, China [c] College of Chemistry and Chemical Engineering, Yangzhou University, Yangzhou, China

Online publication date: 01 December 2009

To cite this Article Yan, Hui , Chu, Liang T. , Jin, Ronghua and Diao, Guowang(2009) 'Studies of Atmospherically Relevant Reactions Using Differentially Pumped Mass Spectrometer and Fourier Transform Infrared Spectroscopy', Spectroscopy Letters, 42: 8, 444 — 457
To link to this Article: DOI: 10.1080/00387010903267146
URL: http://dx.doi.org/10.1080/00387010903267146

Spectroscopy Letters, 42:444–457, 2009

ISSN: 0038-7010 print/1532-2289 online
DOI: 10.1080/00387010903267146

Taylor & Francis
Taylor & Francis Group

Studies of Atmospherically Relevant Reactions Using Differentially Pumped Mass Spectrometer and Fourier Transform Infrared Spectroscopy

Hui Yan[1], Liang T. Chu[1], Ronghua Jin[2], and Guowang Diao[3]

[1]Wadsworth Center, New York State Department of Health and Department of Environmental Health Sciences, School of Public Health, SUNY–Albany, Albany, New York, USA
[2]Department of Chemistry, Shanghai Normal University, Shanghai, China
[3]College of Chemistry and Chemical Engineering, Yangzhou University, Yangzhou, China

ABSTRACT This article describes recent studies of atmospherically relevant reactions using spectroscopic techniques by our group at the Wadsworth Center. Heterogeneous reactions of SO_2 with either HOBr or HOCl on ice have been studied using a coated-wall flow reactor coupled with differentially pumped quadrupole mass spectrometer, and the reaction of NO_2+HI has been investigated using Fourier transform infrared spectroscopy (FTIR). Reaction probabilities or rate constants have been determined at relevant atmospheric temperatures. Specular reflection-absorption infrared spectroscopy and the temperature programmed desorption technique were employed to study the adsorption of oxalic acid on a Cu surface at 175 K. Reflection-absorption infrared spectroscopy showed that oxalic acid is molecularly adsorbed on the Cu surface. The results obtained from these studies provide a better understanding of atmospheric reactions at a molecular level and enable an assessment of the relative importance of the reactions in the atmosphere.

KEYWORDS adsorption, copper surface, heterogeneous reactions, HI, HOBr, HOCl, HONO, ice, NO_2, oxalic acid, quadrupole mass spectrometry, reaction probability, reflection-absorption infrared spectroscopy, sulfur oxidation, temperature programmed desorption, troposphere

INTRODUCTION

Since the discovery of the Antarctic ozone hole, heterogeneous chlorine and bromine chemistry has become a focus of attention in efforts to understand the nature of the polar ozone depletion.[1] Scientific interest in heterogeneous chemistry involving ice or ice-like particles has grown rapidly. Extensive atmospheric field measurements and laboratory studies have been conducted to verify the roles of bromine and chlorine heterogeneous chemistry occurring on the polar stratospheric clouds that are composed of water-ice, HNO_3 hydrates, and supercooled ternary solution.[2–5] It has also

Received 7 September 2007; accepted 15 February 2008.

Address correspondence to Liang T. Chu, Wadsworth Center, New York State Department of Health and Department of Environmental Health Sciences, School of Public Health, SUNY-Albany, P. O. Box 509, Albany, NY 12201-0509. E-mail: lchu@albany.edu

been discovered that heterogeneous reactions occurring on ice and sea-salt particles play a critical role in the Arctic boundary layer ozone loss.[6,7] Reactive halogen species have a profound effect on the boundary layer ozone loss through a generally accepted Br-catalyzed destruction mechanism.[8–10] The central role of these heterogeneous reactions is to convert photochemically inactive halogen compounds into photochemically active forms, which can destroy ozone molecules via catalytic cycles. The repartitioning of active/inactive halogen species in the atmosphere depends on many factors, and the process can be very complicated, especially when compounds from different families are coupled with one another. The process can involve acidic molecules (e.g., SO_2), organic compounds, and even radicals.[11,12] For instance, HOBr and HOCl were suggested to oxidize S(IV) to S(VI), producing sulfate over the ice sea-salt aerosols.[13] The product, sulfate, alters the aerosol properties, thereby affecting heterogeneous bromine and chlorine activation processes. On the other hand, the activated Br can be reduced by oxalic acid over snow/ice surface in the Arctic boundary layer.[14] Thus, it is important to determine kinetics and mechanisms of all relevant reactions in order to model and assess atmospheric processes accurately.

The oxidation of S(IV) to S(VI) is of great importance due to the toxicity and the environmental effects of sulfate, since a large fraction of atmospheric sulfate reaches the ground by deposition as well as by acid rain and snow. The major oxidation pathways are gas-phase OH oxidation and the H_2O_2 aqueous-phase heterogeneous process.[15] In the Arctic boundary layer, atmospheric chemistry modeling work suggests that >60% of S(IV) is oxidized by HOX (X = Br or Cl) over the deliquesced ice-sea salt aerosols.[13] In order to assess the role of this reaction in S(IV) oxidation and halogen activation, it is necessary to determine how rapidly SO_2 can be oxidized by HOBr or HOCl molecules on water-ice or ice-sea salt particle surfaces in the marine boundary layer (MBL).

Oxalic acid, $C_2H_2O_4$, is the most abundant dicarboxylic acid in tropospheric aerosols, and it has been found as an aerosol-borne product of the degradation of hydrocarbons.[16] It is present in both the aerosols and snowpack and can be decomposed by bromine, as suggested by field studies.[14] Oxalic acid exists as oxalate at the mineral-aqueous phase interface.[17] However, the uptake/adsorption behaviors at the gas-surface interface are not known at atmospherically relevant conditions. Whether the adsorbed complex of oxalic acid near aerosol surfaces is in the molecular or ionic state remains to be determined. Thus, an understanding of the adsorption behaviors of oxalic acid on a substrate (e.g., Cu) will provide a necessary preliminary answer to this question.

A number of spectroscopic techniques have been successfully employed to solve environmental chemistry problems such as those above. Quadrupole mass spectrometry (QMS), coupled with use of a coated-wall flow reactor, molecular diffusion tube,[18,19] or Knudsen cell,[20–22] is a common technique to study heterogeneous reactions *in situ* due to the method's high sensitivity and flexibility. Fourier transform infrared spectroscopy (FTIR),[23] coupled with the droplet train apparatus,[24] smog chamber, or White cell,[25,26] is another methodology to investigate reaction kinetics. Tunable IR diode laser absorption spectroscopy is also used to study heterogeneous reactions.[27] Finally, reflection-absorption infrared spectroscopy (RAIRS) is a surface-specific technique to study adsorbed species on metal surfaces and on thin film surfaces over metal substrates.[5,28–32]

The purpose of this article is to illustrate how various spectroscopic techniques have been used by our research group at the Wadsworth Center to obtain chemical kinetic data under atmospherically relevant conditions and to identify the adsorption processes. Two experimental approaches, entailing: (1) a coated-wall flow reactor coupled with a differentially pumped QMS and (2) specular RAIRS in combination with temperature programmed desorption (TPD), are described to illustrate the spectroscopic techniques used. In the following sections, the experimental apparatus used to conduct these studies is described first. Second, results obtained from recent studies are presented to exemplify applications of spectroscopic techniques in atmospheric chemistry. These include: (1) determination of the reaction probabilities for the two heterogeneous reactions $HOBr + SO_2$ and $HOCl + SO_2$ on ice surfaces, (2) adsorption of oxalic acid on a Cu surface, and (3) determination of rate constants for the reaction of $NO_2 + HI$. These studies provide useful kinetic

information on halogen chemistry occurring in the boundary layer and reveal the nature of heterogeneous reactions on snow/ice or ice particle surfaces.

MATERIALS AND METHODS

Instrumentation

QMS with Coated-Wall Flow Reactor

The reaction probability measurements were performed in a coated-wall flow reactor coupled with differentially pumped QMS (Extrel, C50 electronics, Pittsburgh, PA, USA).[33–35] The experimental apparatus is shown in Fig. 1. The flow reactor and QMS vacuum system were interfaced with a flexible stainless-steel bellows and were separated by a valve. The double-jacketed cylindrical flow reactor was made of Pyrex glass. Its dimensions were 35 cm in length and 1.70 cm in inner diameter. The outer jacket was a vacuum layer to maintain the temperature of the reactor. The temperature of the reactor was regulated by a liquid-nitrogen-cooled methanol circulator (Neslab, Newington, NH, USA) and was measured with a pair of J-type thermocouples located in the middle and at the downstream end of the reactor. During the experiment, the temperature was maintained at a temperature in the range of 190–240 K; the stability of the temperature was better than ±0.3 K for every measurement. The pressure inside the reactor (typically 1 Torr) was controlled by a downstream throttle valve (MKS Instruments; Model 651C, Andover, MA, USA) and was measured with a high-precision Baratron pressure gauge (MKS Instruments; Model 690A, Andover, MA, USA); the stability of the pressure was better than 0.005 Torr in every experiment. A double-capillary movable injector was used to admit reactants, such as HOCl and SO_2, into the flow reactor during the reaction probability measurements. The injector was sealed to the reactor by a compression fitting with vacuum grease. To avoid condensation of water vapor and reactants on the capillary wall at low temperature, room-temperature dry air was passed through the outside of the capillary to keep it warm.

RAIRS Combined with RGA

This method combining specular RAIRS with the use of a residual gas analyzer (RGA) (Pfeiffer; Prisma QME 200, Nashua, NH, USA) was designed to determine *in situ* structures of adsorbed complex and desorption kinetics of oxalic acid on a Cu surface.

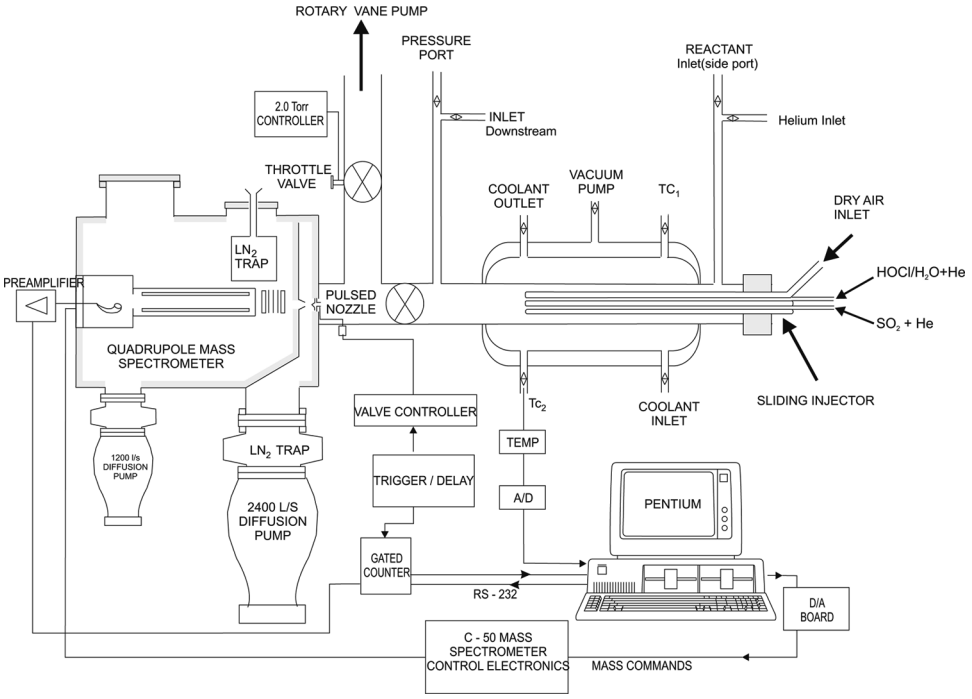

FIGURE 1 **Schematic diagram of the differentially pumped QMS interfaced with a coated-wall flow reactor. The sliding injector with double capillary inlets was used to deposit ice on the wall of the flow reactor and to admit reactants (e.g., HOCl and SO_2) into the reactor. A QMS, housed in the ultra-high vacuum chamber with a base pressure of 6×10^{-11} Torr, was employed to monitor the concentration of reactants and products before, during, and after the reaction or uptake.**

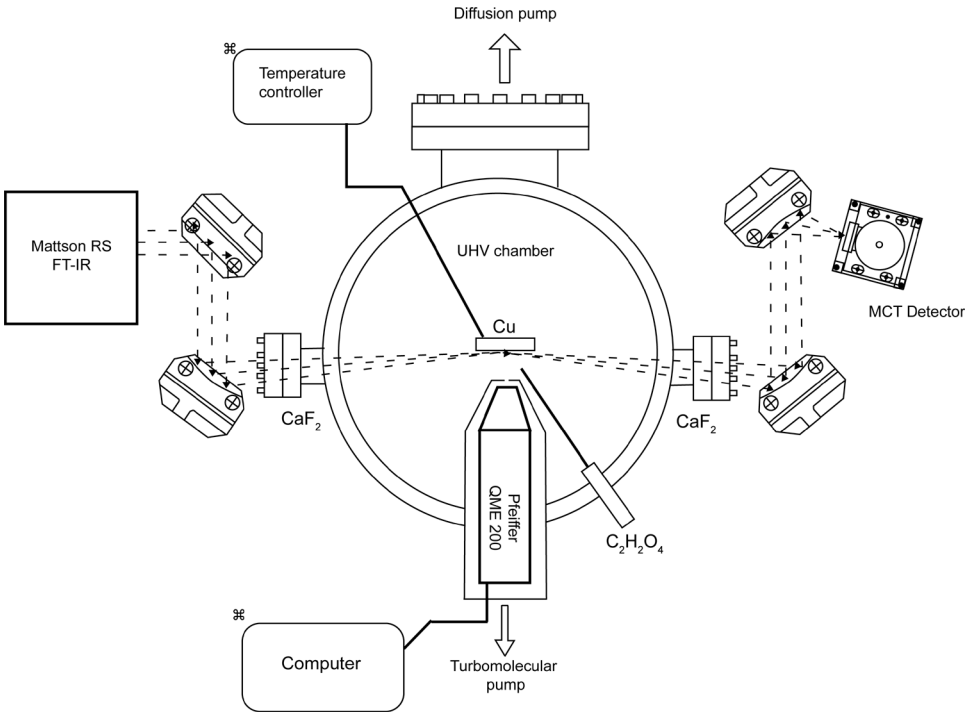

FIGURE 2 **Schematic diagram of the RAIRS-TPD apparatus. The IR beam was redirected from the Mattson RS-1 FTIR onto a polished Cu surface with an incident angle of 85 degrees. The IR absorption by oxalic acid was detected by a liquid nitrogen-cooled narrow-band MCT detector. The Cu surface was cooled by liquid nitrogen and heated using a polyimide heater to achieve the desired temperature. The substrate temperature was programmed to either be maintained at a constant value or to linearly ramp using a temperature controller. A Pfeiffer RGA was used to monitor oxalic acid molecules desorbed from the Cu surface. Oxalic acid was dosed onto the Cu surface by means of a precision leak valve.**

The combination of RAIRS and an RGA allowed the correlation of the desorbed gas-phase products with the appearance/disappearance of adsorbates or structural changes of surface species. A schematic diagram of the apparatus is shown in Fig. 2. The experiments were carried out in a bakeable ultrahigh vacuum (UHV) chamber with a base pressure $<1 \times 10^{-9}$ Torr. An optical-grade Cu disk, 2.5 cm in diameter, was mechanically polished to produce a mirror-smooth surface and was mechanically secured on an X-Y-Z with rotation manipulator (MDC; Model PSM-1502, Hayward, CA, USA) to the vacuum chamber. The FTIR spectrometer (Mattson; Research Series RS-1, Madison, WI, USA), coupled with an external narrow-band HgCdTe (MCT) detector (750–7800 cm^{-1}) with the specular reflection-absorption accessory (Mattson), was located outside the UHV chamber. The FTIR spectrometer was interfaced to the UHV chamber through two differentially pumped CaF_2 windows (McAllister; DPW275, Coeur d'Alene, ID, USA), which were used to provide passage of the IR beam to the sample. The IR beam from the FTIR spectrometer was focused onto the Cu surface, using a 10-inch focal length 90 degree parabolic mirror with an incident angle of 85 degrees. The reflected IR beam was collected by a second identical parabolic mirror and then focused on the MCT detector. The optical pathway is illustrated in Fig. 2 by the dashed lines. The acrylic housing for the optical pathway outside the UHV chamber was sealed and purged with dry N_2 gas to minimize spectral interferences due to CO_2 and H_2O vapor in air.

The RGA was housed in a UHV adaptor and pumped separately by a turbo molecular pump (Pfeiffer; Model TMU 071P, Nashua, NH, USA). The RGA-UHV assembly was placed inside the UHV chamber (Fig. 2). The oxalic acid molecules desorbed from the Cu surface were sampled by RGA through a 1.5-mm diameter sampling hole located in front of the adaptor, which was placed approximately 1.5 cm away from the Cu surface to obtain spectra exclusively from the species desorbing from the surface.

RAIR spectra were recorded before and after the dosing of oxalic acid onto the Cu surface, from 1000 cm^{-1} to 4000 cm^{-1} with 8 cm^{-1} resolution and 512 co-added scans, at 175 K. The Cu surface was

cooled to 175 K using liquid nitrogen. The Cu surface can be heated using a Kapton insulated flexible heater (Omega; KHLV Series) placed directly on the back of the Cu disk. The temperature was measured using a T-type thermocouple mechanically clamped on the Cu surface, and the temperature of the Cu surface was controlled by a temperature controller (Omega; Model CN3251). The thermocouple was calibrated in a separate experiment. The background single-beam spectrum was recorded before the dosing of oxalic acid onto the Cu surface, and the sample single-beam spectrum was recorded after the dosing. The RAIR spectra were reported as the ratio of the oxalic acid spectrum to the background spectrum. Once the RAIR spectrum was recorded, the TPD experiment was conducted immediately to investigate the desorption kinetics of oxalic acid from the Cu surface. During the course of the TPD experiment, the surface was heated by the Kapton heater, with a linear heating rate of 5 K–min^{-1}. The RGA, controlled by the Quadstar software (Pfeiffer), was used to monitor oxalic acid molecules and other species desorbing from the Cu surface. The RGA signal was collected at $m/z = 45$ (mass 45 is the major fragment of oxalic acid; the parent peak at $m/z = 90$ is weak[36]). The temperature resolution was approximately 0.6 K, limited by an external 11-bit A/D converter.

Sample Preparations

Ice Films

The ice film was prepared by passing helium carrier gas (BOC; 99.9999%) through a high-purity deionized water (Millipore Milli-Q plus; $> 18\,M\Omega \cdot cm$, Billerica, MA, USA) reservoir, which was maintained at 293.2 ± 0.1 K by a refrigerated circulator (Neslab; Model RTE-100LP). During the course of the ice deposition, helium saturated with the water vapor was introduced to the reactor (maintained at a temperature of the experiment) through an inlet of the double-capillary injector, which was then slowly pulled out at a constant speed to allow a uniform ice film to be formed on the inner wall of the reactor. The amount of ice deposited was determined from the water vapor pressure, the mass flow rate of the helium-water mixture as measured by a Hasting mass flow meter, and the deposition time. The average film thickness h was calculated from the geometric area of the ice film on the flow reactor, the mass of ice, and the bulk density ($\rho_b = 0.63\,g \cdot cm^{-3}$) of vapor-deposited ice.[37]

HOBr and HOCl

The HOBr solution was prepared by adding Br_2 to 2.1% wt $AgNO_3$ solution at 0°C.[38,39] The HOCl solution was prepared by adding 5%wt $AgNO_3$ solution to a diluted NaOCl (Aldrich; 6% active chlorine, Milwaukie, WI, USA) solution.[40] The concentration of the HOBr or HOCl vapor was calibrated by reacting the vapor with HCl or HBr on ice surfaces at 190 K, respectively, according to the reactions $HOBr + HCl(s) \rightarrow BrCl + H_2O(s)$ and $HOCl + HBr(s) \rightarrow BrCl + H_2O(s)$, in separate experiments.[39]

Oxalic Acid

Oxalic acid (Aldrich; 99 + %) was purified by vacuum distillation and sublimation procedures. Oxalic acid was placed in a small glass vessel and was continuously evacuated by a mechanical pump with a liquid nitrogen trap for extended period of time; it was then heated by a water bath at 313 K under vacuum, to sublimate it (oxalic acid decomposed at warmer temperature, and byproducts were observed by the RAIRS). Once the oxalic acid was purified, its vapor was admitted onto the Cu surface using a UHV precision leak valve (MDC; Model ULV-150). The amount of oxalic acid adsorbed on the Cu was determined through a TPD experiment (see the Results and Discussion section).

RESULTS AND DISCUSSION

Heterogeneous Reactions of $HOX + SO_2$ on Ice Surfaces

Oxidation of S(IV) by HOBr or HOCl over ice-sea salt surfaces in the MBL is suggested by atmospheric chemistry modeling calculations.[13,41] Both HOBr and HOCl have been shown to oxidize S(IV) in solution.[42–44] Prior to previous studies,[38,40] there were no published experimental investigations of these reactions on ice surfaces. The heterogeneous reactions of SO_2 with HOBr or HOCl on ice surfaces were investigated, and the reaction probability γ was determined. γ is defined as the ratio of the number of collisions for SO_2 molecules that lead to the reaction to the total number of SO_2 molecules colliding with the HOX-ice surface (X = Br or Cl).

A 20-cm length of ice film was first prepared by water vapor deposition on the inner wall of the flow reactor for every measurement. Second, the helium carrier gas was bubbled through the HOCl solution, which was kept at 273.2 K (HOCl was used in this case to illustrate the experiment). The HOCl vapor-He mixture was then admitted to one inlet of the double capillary injector, and the SO_2–He mixture was admitted to the other inlet of the injector simultaneously. Before SO_2 reacted with HOCl on the ice film, both initial SO_2 and HOCl signals were determined by the QMS. SO_2 was monitored by the QMS at m/z = 64 and HOCl at m/z = 52. After both SO_2 and HOCl signals were stabilized, the sliding injector was slowly pulled out toward the upstream end of the flow reactor in 2-cm increments. A typical QMS signal for SO_2 loss on an ice surface with concurrent flow of HOCl, as a function of reaction time, is shown in Fig. 3. The typical data acquisition time was 10–30 s per point. The surface coverage of HOCl was determined by integration of the calibrated HOCl signal over the exposure time. For the pseudo first-order rate under the plug-flow conditions, the following relationship holds for SO_2:

$$\ln[SO_2]_z = -k_s(z/v) + \ln[SO_2]_0, \qquad (1)$$

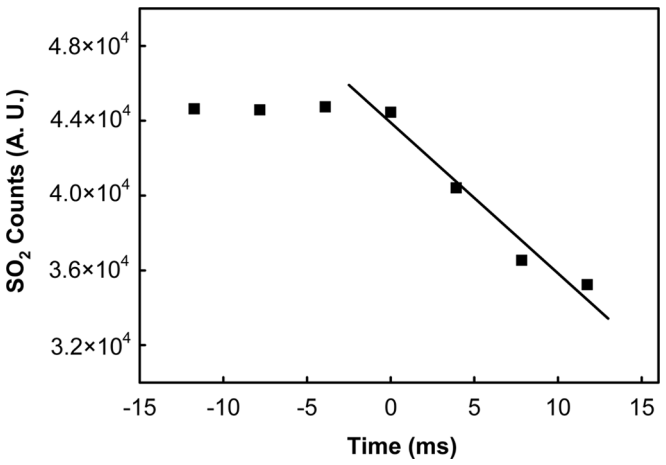

FIGURE 3 **Plot of the log SO_2 signal versus the reaction time (z/v) on an HOCl-ice film at 190 K. (■) represents the SO_2 QMS signal for the concurrent flows of SO_2 and HOCl over the ice-film surface. The plot shows the initial SO_2 signal before the SO_2 came in contact with the ice ($t < 0$) and the subsequent loss of SO_2 on the HOCl-ice film surface. The background SO_2 signal was corrected. The pseudo first-order rate constant was determined to be $k_s = 20.4 \pm 2.0\ s^{-1}$, and $k_w = 21.1 \pm 2.1\ s^{-1}$. The initial reaction probability is $\gamma_w = (1.4 \pm 0.2) \times 10^{-3}$, $PSO_2 = (1.45 \pm 0.05) \times 10^{-6}$ Torr, $P_{HOCl} = 4.2 \times 10^{-6}$ Torr, the total pressure is 1.000 ± 0.005 Torr, the mean flow velocity, ν, is $5.5\ m \cdot s^{-1}$, and the ice film thickness is 3.3 μm.**

where z is the injector position, v is the mean flow velocity, $[SO_2]_z$ is the gas-phase SO_2 concentration measured by the QMS at position z, and the subscript 0 denotes the initial injector reference position. The pseudo first-order loss rate constant, k_s, was determined from the least-squares fit of the experimental data to Eq. (1). A value of $k_s = 20.4 \pm 2.0\ s^{-1}$ was obtained for $SO_2 + HOCl$ at 190 K. k_s was then corrected for the gas-phase axial and radial diffusion using a standard procedure,[45] and the corrected rate constant was termed k_w. A diffusion coefficient for SO_2 in helium was estimated to be $160\ cm^2 \cdot s^{-1} \cdot Torr^{-1}$ at 190 K and 1.0 Torr.[46,47] The reaction probability γ_w was calculated from k_w using the following equation:[48,49]

$$\gamma_w = 2R\ k_w/(\omega + R\ k_w), \qquad (2)$$

where R is the radius of the flow reactor (0.85 cm), and ω is the mean SO_2 molecular velocity at the ice-film temperature.

Measurements of the reaction probability as a function of ice-film thickness indicate that the vapor-deposited ice film is porous and has internal surface areas.[37] On the basis of the results of previous studies conducted under similar conditions,[50,51] ice films can be approximated as hexagonally close-packed spherical granules stacked in layers.[52] The internal surface area of the ice film can be corrected. The corrected reaction probability is called the "true" reaction probability, γ_t. γ_t is related to the value γ_w by

$$\gamma_t = \frac{\sqrt{3}\gamma_w}{\pi\{1 + \eta[2(N_L - 1) + (3/2)^{1/2}]\}}, \qquad (3)$$

where the effectiveness factor, $\eta = \phi^{-1}\tanh\phi$, is the fraction of the film surface that participates in the reaction (η is a function of γ_t) $\phi = \left((N_L - 1)\left(\frac{2}{3}\right)^{1/2} + \left(\frac{1}{2}\right)\right)\left[\frac{3\rho_b}{2(\rho_t - \rho_b)}\right](3\tau\gamma_t)^{1/2}$, where ρ_t and ρ_b are the true density and bulk density of the ice, τ is tortuosity factor, and N_L is the number of granule layers.[49,52] A tortuosity factor $\tau = 4$ and true ice density $\rho_t = 0.925\ g \cdot cm^{-3}$ were used to solve γ_t using combined Eq. (3) and η.[40] The reaction of SO_2 and HOBr followed the same procedures as that of SO_2 and HOCl, only with the HOBr monitored by QMS at m/z = 96; details can be found in reference.[40]

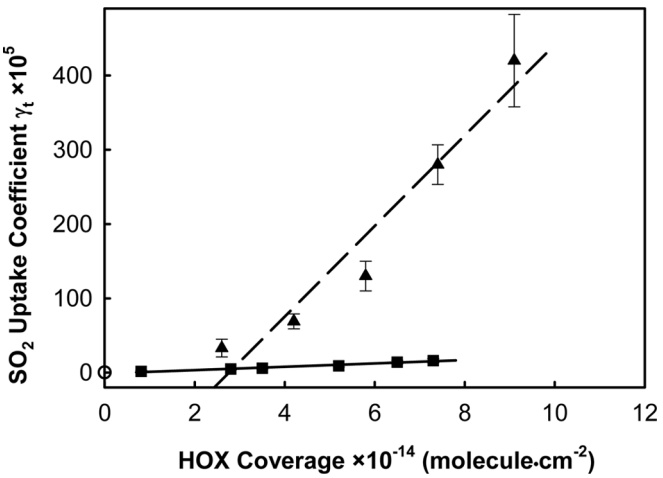

FIGURE 4 Plot of the true reaction probability of SO_2, γ_t, versus HOX surface coverage. (▲) is γ_t on ice films with the concurrent flows of SO_2 and HOBr at 190.1 ± 0.5 K, and (■) is γ_t on ice films with the concurrent flows of SO_2 and HOCl at 190.0 ± 0.7 K. The error bars include both one standard deviation $\pm\sigma$ of the mean value and systematic errors. (○) is the γ_t value of SO_2 on ice. The lines were fitted to the Eley-Rideal mechanism. The thickness of ice films is 3.3 ± 0.3 μm.

The reaction probability for SO_2 with HOBr or HOCl on ice films was studied as a function of surface coverage of corresponding HOX. Figure 4 shows that mean γ_t is a function of either HOBr or HOCl surface coverage (molecule $\cdot$ cm^{-2}) at 190 K for the respective reactions $SO_2 + HOBr$ and $SO_2 + HOCl$. Figure 4 shows that the γ_t value increases from 1.6×10^{-5} to 1.6×10^{-4} as the HOCl surface coverage increasing from 8.1×10^{13} to 7.3×10^{14} molecule $\cdot$ cm^{-2}; the γ_t value increases from 3.3×10^{-4} to 4.2×10^{-3} for an HOBr surface coverage increasing from 2.6×10^{14} to 9.1×10^{14} molecule $\cdot$ cm^{-2} at 190 K[40] under the condition of concurrent flow of SO_2 and HOX on ice surfaces. Clearly, these values are higher than the γ_t value of SO_2 on ice surfaces, 2.0×10^{-6} (Fig. 4), at the same temperature, suggesting that the loss of SO_2 on the snow/ice surface is enhanced by the presence of either HOBr or HOCl. At a given surface coverage, (e.g., 5×10^{14} molecule $\cdot$ cm^{-2}), γ_t of SO_2 on HOBr-ice is approximately one order of magnitude higher than γ_t on HOCl-ice.

The experimental observations (both reactions) can be described using the Eley-Rideal mechanism, $\gamma_t = k_b \theta_{HOX}$, where k_b is the overall rate constants and θ_{Hox} is the surface coverage of HOX.[40] The k_b values were determined from the slope of the fit (lines in Fig. 4) to be 6.1×10^{-18} and 2.3×10^{-19} molecule$^{-1} \cdot$ cm^2 at 190 K[40] for the reactions of SO_2 with HOBr and HOCl, respectively. The data for the reaction of $SO_2 + HOBr$ are not well represented by the fitted line at low HOBr coverage. This is due to the approximations used to derive the mechanism.[40] The higher k_b value for the SO_2 reaction with HOBr than that of the SO_2 reaction with HOCl on ice surfaces can be explained on the basis of the Lewis acid-base theory.[40] The reaction probability for SO_2 with HOCl on ice films was also determined as a function of temperature. $\gamma_t = 3.4 \times 10^{-15}$ exp $(4.45 \times 10^3/T)$ at 190–238 K. It shows that γ_t decreases exponentially as the temperature increases.

This study shows that SO_2 uptake is enhanced by the presence of HOX on ice, due to its reactivity toward HOX, relative to the rate of SO_2 uptake on ice at 190 K. The SO_2 reaction with HOBr is more rapid than the analogous reaction with HOCl on ice surfaces at 190 K. However, the γ value of the SO_2 reaction with HOCl on ice at the MBL temperature (>230 K) is comparable to the γ of SO_2 on ice. Also, if HOBr or HOCl coverage is depleted in the boundary layer, the nature of the reactions changes; it becomes the loss of SO_2 on water-ice. Thus, SO_2 oxidation by HOBr and HOCl is not expected to be a significant pathway in the MBL.

Adsorption and Desorption of Oxalic Acid on a Cu Surface

Atmospheric field measurements have shown that a variety of organic acids exist in both the gas phase and the particle phase. The predominant organic acids found in the gas phase are formic acid and acetic acid. A variety of dicarboxylic acids, such as oxalic acid and malonic acid, are also found in air.[11] However, due to low vapor pressures of dicarboxylic acids, these acids are found predominantly in the particle phase. Thus, dicarboxylic acids have an influence on the chemical and physical properties of aerosols. Oxalic acid/oxalate adsorbed on mineral surfaces was studied using attenuated total reflectance FTIR.[17,53] Martin et al. have studied adsorption of oxalic acid, as a hydrogen oxalate, on a Cu(110) surface at 300 K and 370 K.[54] They employed both RAIRS and reflection anisotropy spectroscopy to identify the adsorbed complexes.

Ice is a common material in the terrestrial environments and is one of the major components in aerosols. The interaction between oxalic acid and ice is

important in tropospheric chemistry. In order to understand the nature of the adsorption/interaction of oxalic acid on ice surfaces at atmospherically relevant temperatures, the adsorption of oxalic acid on a Cu substrate surface using RAIRS at 175 K is investigated. Cu is chosen as the substrate because of its high IR reflectivity, which is critical in a RAIRS analysis,[28] and its good thermal conductivity. This is the first stage of our study seeking to understand the adsorption of oxalic acid on ice.

Oxalic acid was dosed on the Cu surface after the Cu surface had been cooled down to 175 K, and the RAIR spectrum was recorded. A typical RAIR spectrum of oxalic acid (8 Langmuir) adsorbed on a Cu surface at 175 K is shown in Fig. 5. The bands with high absorption intensities in the spectrum demonstrate the presence of adsorbed oxalic acid. On the basis of previous IR studies of crystalline oxalic acid,[55–57] and hydrogen oxalate on Cu(110),[54] the following vibrational modes have been assigned to the bands depicted in Fig. 5. The strong absorption feature, from 1700 to 1800 cm^{-1}, labeled as 1770 cm^{-1}, is attributed to carboxylic stretching mode, νC=O. Vibrational bands at 1335, 1270, and 1225 cm^{-1} are associated with two different modes, namely δCOH and νC–O modes.[54–57] Weaker intensity and higher frequency δCOH modes are difficult to identify in the spectrum due to the gas-phase H_2O absorption in the same region; they were not labeled in the spectrum. A broad OH band, observed in the range of 2780 to 3450 cm^{-1} and peaking at approximate 3110 cm^{-1}, is probably due to hydrogen bonds among oxalic acid molecules in the same layer or from the neighboring layers (intramolecular hydrogen bonds are also possible).[54,55,57] The broad OH band is also found in an IR spectrum of crystalline oxalic acid. Oxalic acid has two crystalline phases, α and β, and hydrogen bonds exist in both phases. In the α-phase, the C=O and OH groups of a single COOH are each hydrogen-bonded with a different oxalic acid molecule to form a planner sheet structure, and a broad band from νO–H mode appears from 2600 to 3400 cm^{-1} centered at 3117 cm^{-1}. In β-phase oxalic acid, in contrast, the molecules are linked together in long chains by cyclic hydrogen bonds, leading to a broad band (νO–H) from 2400 to 3300 cm^{-1} centered at ~3000 cm^{-1}.[55–57] However, it was indeterminable whether the adsorbed multilayer oxalic acid molecules (ultrathin film) belong to the α- or the β-crystalline phase or to a mixture of the two. In addition, the characteristic bands of oxalate, ~1650 cm^{-1} for the asymmetric ν_{as}OCO mode and 1420 cm^{-1} for the symmetric ν_sOCO mode,[54] are absent from the spectrum, suggesting that oxalic acid is molecularly adsorbed (multilayer) on the Cu surface. A doublet-structured peak centered at ~2350 cm^{-1} is due to gas-phase CO_2 absorption, and other structural bands from 1450 to 1750 cm^{-1} and 3550 to 3950 cm^{-1} are attributed to the gas-phase H_2O absorption.[36] The trace amounts of gas-phase CO_2 and H_2O are likely present in the optical path outside the vacuum chamber, despite the continuously purging of the entire optical pathway with dry nitrogen gas.

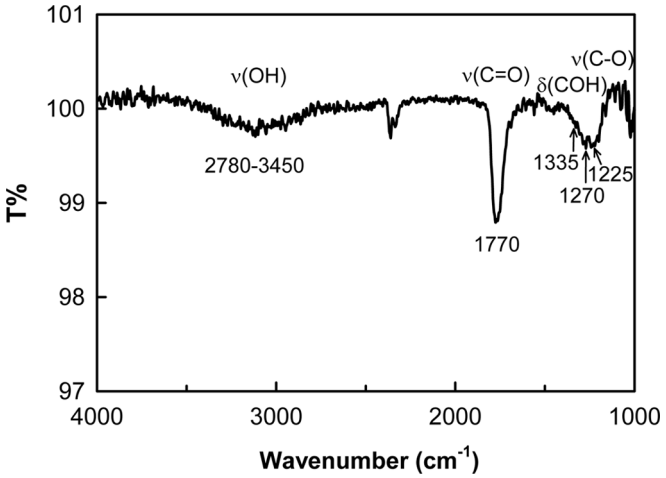

FIGURE 5 **A RAIR spectrum of oxalic acid on a Cu surface at 175 K. The surface coverage of oxalic acid is about 8 L (1 L = 10^{-6} Torr·s). Bands at 2780–3450 cm^{-1} are attributed to νOH; bands labeled as 1770 cm^{-1} are the vibrational modes of νC=O; and bands at 1335, 1270, and 1225 cm^{-1} belong to the vibrational modes of δCOH and νC–O. The cut-off frequency is ~1000 cm^{-1} due to the CaF_2 windows on the apparatus.**

In order to clarify the structure of the oxalic acid complex adsorbed on the Cu surface, as well as the nature of the adsorption process, a TPD experiment was performed. Oxalic acid vapor was dosed on the Cu surface at 175 K, and the sample was then resistively heated. Figure 6 shows a typical desorption profile of 8 Langmuir (L = 10^{-6} Torr·s) oxalic acid from the Cu surface with a linear heating rate of 5 K·min^{-1} from 175 K to 283 K. The desorbed oxalic acid signal (m/z = 45) was collected by the RGA, and the temperature was measured by a T-type thermocouple clamped on the Cu surface. The TPD spectrum shows two desorption peaks, at 222 K (shoulder) and 245 K, suggesting that oxalic acid adsorbs on the Cu surface with multiple adsorption

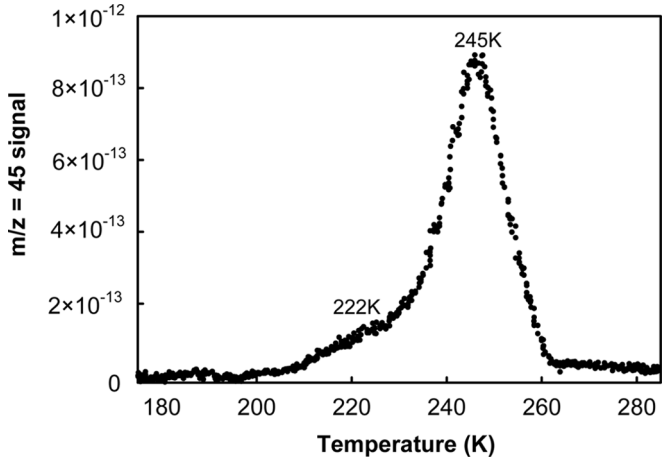

FIGURE 6 **TPD spectrum of oxalic acid with 8-L coverage from the Cu surface. The Cu surface was heated at $5\,K \cdot min^{-1}$ from 175 K to 283 K, and the gas-phase oxalic acid signal (ion current) was then collected by RGA (m/z = 45). The TPD profile shows two desorption peaks at 222 K (shoulder) and 245 K, suggesting that oxalic acid has two possible adsorption sites and that oxalic acid is desorbed from Cu at T > 245 K.**

sites. In a series of TPD experiments (Fig. 7), the oxalic acid surface coverage was varied from ~1 L to 20 L and then recorded desorption profiles. At low coverage (i.e., ~1 L), where oxalic acid is expected to be adsorbed on the Cu surface as a monolayer, the TPD spectrum shows a low-temperature shoulder peak (222 K) only, suggesting that the shoulder peak is associated with the surface-layer adsorbed oxalic acid. As the surface coverage

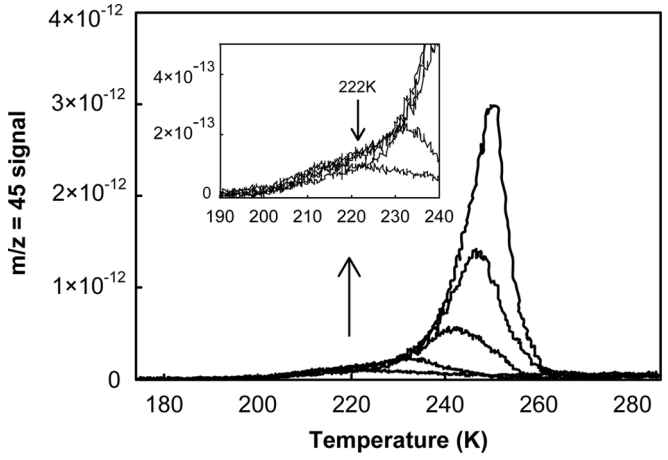

FIGURE 7 **TPD spectra of oxalic acid on the Cu surface. Oxalic acid was deposited on the Cu surface with varying surface coverages, from ~1, 2.9, 8.8, 12, and to 20.5 L, at 175 K. The plots show that, at low coverage (~1 L), there is a shoulder peak. As the coverage increases, a second desorption peak appears at ~245 K. The desorption temperature for the second desorption peak increases with the surface coverage. The insert plot shows that the desorption temperature of the shoulder peak (222 K) is independent of the oxalic acid surface coverage.**

of oxalic acid increases, the desorption temperature of the shoulder peak remains unchanged, and so does the peak intensity. The surface-layer adsorbed oxalic acid is independent of the α- or β-phase of oxalic acid. The 245 K peak position, in contrast, shifts toward a higher temperature and the peak intensity increases, suggesting that more thermal energy is required to desorb multilayer adsorbed oxalic acid from the Cu surface. It is expected that more hydrogen bonding interactions will occur within multilayer structures than in the monolayer, and more energy should be required to separate lateral interactions in the multilayer. Thus, the desorption temperature for the 245 K peak (Fig. 7) shifts toward higher temperatures as the surface coverage increases. The shoulder desorption peak is typical of a film undergoing structural modification on the substrate before sublimation (see discussion below); a similar desorption profile was observed for an acetic acid film on a polycrystalline gold surface.[58] It is considered that the oxalic acid ultrathin film (i.e., multilayer adsorbed oxalic acid) on the Cu surface has defects and/or steps. Oxalic acid, either at the surface layer of the ultrathin film or at defects, experiences fewer hydrogen bonding/lateral interactions (i.e., fewer hydrogen bonds on the surface layer than crystalline oxalic acid) and should be considered to be composed of weakly bonded molecules.

During the heating processes, either these oxalic acid molecules undergo structural modification to form a relatively highly ordered crystalline-like ultrathin film, or else a small proportion of them desorb to the gas phase, which appears as a shoulder peak in the spectrum. Then, the multilayer adsorbed oxalic acid desorbs from the Cu surface once the temperature reaches 245 K or above. The desorption temperature of oxalic acid from the Cu surface is similar to the desorption temperatures for molecularly adsorbed formic acid on Ru (001) (198 K)[59] and on polycrystalline Au (190 K; also acetic acid [205 K]).[58] Figure 7 also suggests that the energy difference between surface sites and multilayer "bulk" sites is small due to a small temperature difference, ~30 K.

The existence of multiple adsorption sites of oxalic acid was further characterized by the RAIRS analysis, performed simultaneously with the TPD experiment. Figure 8 shows oxalic acid RAIR spectra (8 L) recorded at 175 K, 222 K, 240 K, and 283 K. Spectrum 8a was recorded at 175 K, and spectral

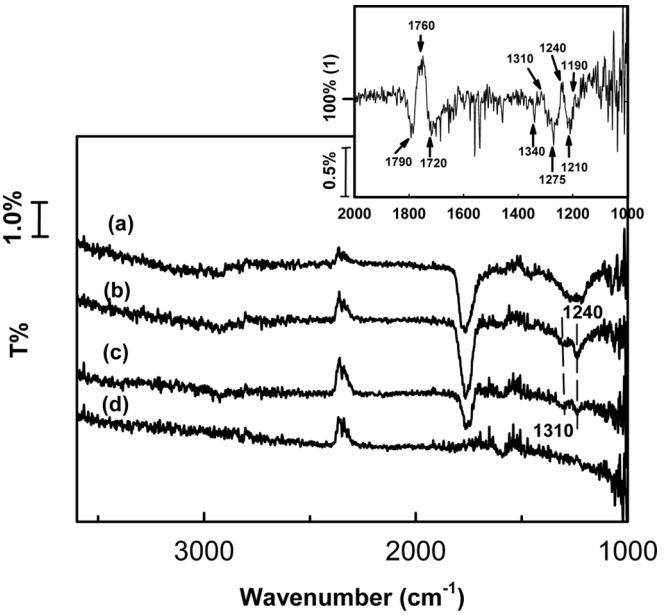

FIGURE 8 **RAIR spectra of oxalic acid on the Cu surface at various temperatures: (a) RAIR spectrum of 8 L oxalic acid on the Cu surface at 175 K and (b) RAIR spectrum at 222 K. After the temperature was ramped from 175 K to 222 K, several bands between 1100 and 1400 cm^{-1} disappeared, and others were shifted to lower wavenumbers. This is illustrated in the insert by a difference spectrum between (a) and (b) (see text for details), (c) The temperature continued to be ramped to 240 K, and the spectrum (c) was recorded at 240 K. The intensities of all bands have decreased, but the frequencies of the bands remain unchanged, (d) At 283 K, which is above the desorption temperature, all bands of oxalic acid have disappeared. Note that no oxalate feature was observed in any of these spectra.**

features are identical to Fig. 5. When the sample was heated to 222 K, spectrum 8b shows that the bands at 1100–1400 cm^{-1}, 1700–1800 cm^{-1}, and 2780–3450 cm^{-1} appear at *lower* frequencies relative to these bands recorded at 175 K (spectrum 8a). When we subtracted spectrum 8b from spectrum 8a, a difference spectrum was obtained, shown as the inserted figure. The absorption intensity differs slightly between spectra 8a and 8b (it was not corrected obtain the difference spectrum); the difference spectrum shows bands with the transmittances both greater and less than 100%. The difference spectrum shows four bands with transmittance > 1, centered approximately at 1760, 1310, 1240, and 1190 cm^{-1} (bands with very weak absorbance are not labeled); these correspond to the bands in spectrum 8b. The difference spectrum also shows five bands with transmittance < 1, centered approximately at 1790, 1720, 1340, 1275, and 1210 cm^{-1}. These bands are absent from spectrum 8b. It is necessary to point out that the vibrational frequencies of these bands (transmittance < 1) are higher than the frequencies of bands with transmittance > 1. These bands can be associated with those oxalic acid molecules that are adsorbed on the surface layer of the ultrathin film and/or on defects of the film (perhaps from internal surfaces). C=O and COOH groups in oxalic acid adsorbed on the surface layer or surface defect sites experience fewer hydrogen-bonding and lateral interactions than do the groups in oxalic acid in the multilayer bulk sites. Their vibrational frequencies (e.g., 1790 cm^{-1}) are higher than those of the functional groups in the bulk of the multilayer. When the multilayer oxalic acid film is heated, the surfaces are annealed, and defects are reduced (structural modification). Bands with stronger intermolecular interaction were observed: bulk-like oxalic acid with massive hydrogen bonds in spectrum 8b coupled with the lower vibrational frequencies (e.g., 1760 and 1310 cm^{-1}) as the result of the desorbing away of surface-bound oxalic acid (e.g., the corresponding modes are 1790 and 1340 cm^{-1}). Additionally, the absorption intensities at 1760, 1310, and 1240 cm^{-1} in spectrum 8b are higher and the bandwidth is narrower relative to spectrum 8a, suggesting a structural modification of less well-ordered multilayer oxalic acid into relatively more highly ordered α- and/or β-like crystalline oxalic acid multilayer. When the temperature was ramped to 240 K (spectrum 8c), the absorption intensities of bands decreased, but the frequencies of bands remained unchanged relative to spectrum 8b taken at 222 K, suggesting that the desorbed species come from the same adsorption site, namely, the bulk multilayer. At 283 K, which is above the desorption temperature, all bands disappeared (spectrum 8d). It is important to point out that we did not observe any bands at $\sim$1420 cm^{-1}, associated with ν_sOCO stretching, or at $\sim$1650 cm^{-1}, associated with ν_{as}OCO stretching, under experimental conditions, suggesting that no oxalate was formed during the TPD experiment. Therefore, it is confirmed that oxalic acid exists as a molecularly adsorbed multilayer on the Cu surface. Combined with the TPD results, this suggests that the ultrathin oxalic acid films undergo structural modification, as indicated by a loss of higher vibrational frequency surface-layer oxalic acid before sublimation.

The bulk-like oxalic acid has more hydrogen bonding/lateral interactions and results in lower vibrational frequency and higher desorption temperature.

Oxalic acid surface coverage on the Cu surface was determined using a TPD approach. The amount of oxalic acid adsorbed on the Cu surface is assumed to be equal to the total amount of oxalic acid desorbed from the surface, which is measured by TPD. The oxalic acid signal intensity in the TPD experiment is determined, in a separate experiment, as follows. First, the total pressure of the UHV chamber was measured with an ionization gauge (Varian Multi-Gauge, Bayard-Alpert, Lexington, MA, USA). The partial pressures of individual components, Ar, H_2O, CO/N_2, and CO_2, in the UHV chamber were determined based on the sensitivity factors of the Pfeiffer RGA. The background pressure of oxalic acid, P_b (Torr), was obtained by the subtraction of the partial pressures of individual components from the total pressure; the RGA signal at $m/z = 45$ was recorded as I_b. Second, the oxalic acid vapor was backfilled into the room-temperature UHV chamber (oxalic acid is not expected to adsorb on the Cu surface at room temperature). The oxalic acid pressure P_s and signal I_s were determined using the procedure outlined above.

Once we subtract the background pressure of oxalic acid from the measured partial pressure, the net oxalic acid partial pressure, $(P_s - P_b)$ is determined, and the corresponding change of the RGA signal at $m/z = 45$ $(I_s - I_b)$ is also obtained. Since 1 Langmuir $= 10^{-6}$ Torr $\cdot$ s, the amount of desorbed oxalic acid can be expressed in Langmuir (L). 1 Langmuir desorbed oxalic acid is equivalent to 1 monolayer (ML) coverage. We can express the measured desorption signal (integrated peak area, A $\cdot$ s) in terms of L or ML using the above calibration $(1\,\mathrm{L} = (2.1 \pm 0.32) \times 10^{-11}\,\mathrm{A \cdot s}$, average of five experiments). It is important to point out that the signals of the RGA collected during the TPD experiments are acquired under identical conditions to those in the calibration experiments, that is, the same emission current, multiplier voltage, and data collection time.

We have investigated the adsorption of oxalic acid on the Cu surface using our RAIRS-TPD apparatus. The combined RAIRS and TPD results show that multilayer oxalic acid is molecularly adsorbed on the Cu surface. Adsorbed oxalic acid undergoes structural modification before it sublimates/desorbs from the Cu surface. It is the invention of the authors to extend this work to study the adsorption of oxalic acid/ice.

Gas-Phase Reaction of $NO_2 + HI$

Like HCl and HBr,[18,33] HI can be adsorbed on snow/ice and aerosols in the atmosphere, and thus, heterogeneous reactions involving HI may play a role in determining the fate of iodine species.[60] One of the relevant heterogeneous reactions involving HI is its reaction with HONO,[61] which is an important trace species in the troposphere, especially above cities.[62]

Since gaseous NO_2 is closely associated with HONO, it is necessary to establish whether NO_2 reacts with HI in the gas phase to produce I_2 directly. Very little was known about the $NO_2 + HI$ reaction prior to previous studies, although the reaction of NO_2 with HCl or HBr over the temperature range 373–693 K was investigated by Rosser and Wise.[63] Determination of the products and kinetics for the $NO_2 + HI$ reaction is critical to an understanding of the nature of the heterogeneous reaction of HONO with HI adsorbed on an ice surface.

Diao and Chu have studied the reaction of $NO_2 + HI$ in a double-jacketed optical cell. The cell had a BaF_2 window on each end. The length of the cell was 17.7 cm, and the inner diameter was 2.05 cm.[64] Both reactants and products were monitored using FTIR (Mattson; Research Series RS-1, Madison, WI, USA). First, gaseous NO_2 was admitted to the cell. Then, the HI gas was expanded into the cell to mix with NO_2. Both the NO_2 and HI concentrations were calibrated.[64] [HI] was controlled > eight-fold higher than $[NO_2]$ to provide a pseudo first-order reaction condition.

Immediately after mixing HI with NO_2 in the cell, IR spectra were recorded as a function of reaction time, *t*. All spectra were recorded at 1 cm^{-1} resolution. A typical set of IR spectra is shown in Fig. 9. A pure NO_2 spectrum, before the reaction, is shown in Fig. 9a. The spectra in Figs. 9b through 9d were acquired at various reaction time points after HI was mixed with NO_2. As the reaction time increases, the intensity of NO_2 bands, centered at 1617 cm^{-1}, decreases; meanwhile, the bands of H_2O and NO, centered at 1875 cm^{-1}, increase in intensity. At 24.5 s, the NO_2 absorption band completely disappears, whereas the intensities for the NO and H_2O peaks reach their maxima. Figure 9b shows additional peaks at 1264, 791, and 852 cm^{-1},[65] suggesting that HONO appears during the reaction.

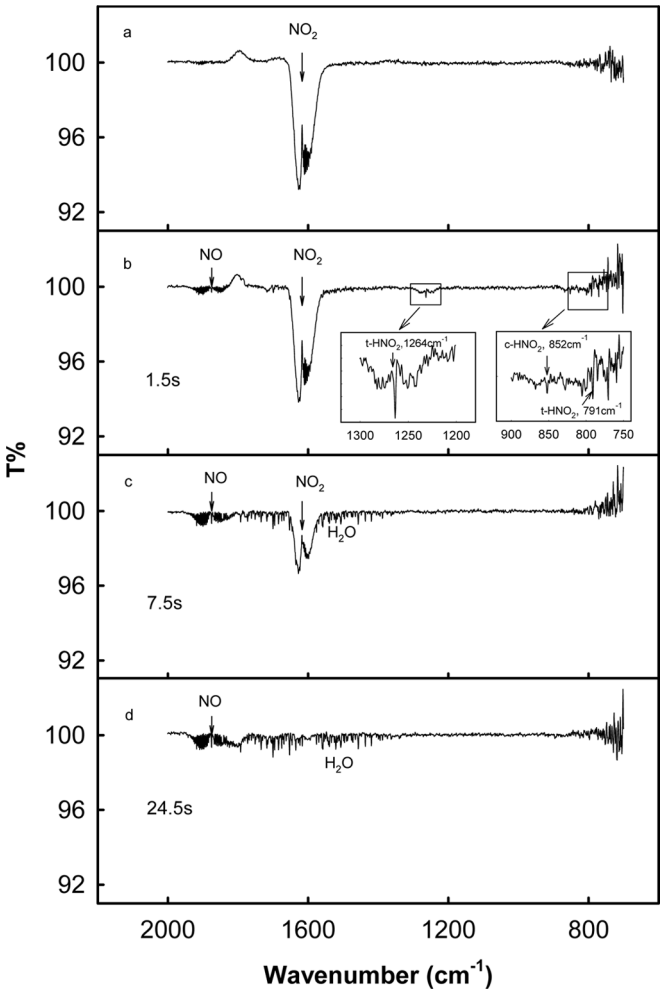

FIGURE 9 **FTIR spectra obtained by reacting NO_2 with HI at 303 K in a double-jacket optical cell. The individual IR spectrum was recorded at reaction time t equals: (a) 0 s, (b) 1.5 s (b), (c) 7.5 s and (d) 24.5 s respectively. $[NO_2]_0 = 6.8 \times 10^{15}$ molecule·cm^{-3} and $[HI]_0 = 5.4 \times 10^{16}$ molecule·cm^{-3}. The temperature was controlled using a refrigerated recirculator. (Adapted from [64] with permission of the PCCP Owner Societies).**

The HONO absorption is below detection level in Figs. 9c and 9d, suggesting that HONO was rapidly formed at the beginning of the experiment and was subsequently consumed by further reactions.

The reaction between NO_2 and HI can be described as $NO_2 + HI \rightarrow$ products. The reaction was determined to be first-order with respect to both NO_2 and HI.[64] Since [HI] is in excess, the rate of the reaction can be written as:

$$-\frac{d[NO_2]}{dt} = k[NO_2][HI] = k_{1st}[NO_2], \qquad (4)$$

where k is a second-order rate constant, $k_{1st} = k[HI]$ is a pseudo first-order rate constant, and $[NO_2]$ and [HI] are the concentrations of NO_2 and HI, respectively. $-k_{1st}$ can be determined from the slope of a plot of log $[NO_2]$ versus t, as shown in Fig. 10. k_{1st} values were also determined as a function of initial HI concentration. On the basis of $k_{1st} = k[HI]$, the second-order rate constant can be deduced from the slope of a plot of k_{1st} versus [HI] to be $k = (6.9 \pm 1.1) \times 10^{-19}$ cm^{-3} · molecule^{-1} at 303 K.[64] The effect of the temperature and heterogeneous effects (wall effects) on the measured rate constants for this reaction can be found in details by Diao and Chu.[64]

On the basis of the product analysis and kinetics, a reaction scheme is proposed. The initiation step $NO_2 + HI \xrightarrow{k} HNO_2 + I$ is followed by a heterogeneous reaction $HNO_2 + HI(s) \rightarrow INO + H_2O$ and a recombination reaction $I + INO \rightarrow I_2 + NO$, so as to produce NO, I_2, and H_2O.[64] HNO_2 was produced during the course of reaction as an intermediate, which was identified using the IR and shown in Fig. 9. Also, NO was identified. However, the reaction $NO_2 + HI \rightarrow$ products is unlikely to play a major role in the removal of HI in the atmosphere due to its slow rate, compared to the major gas-phase HI removal pathways that operate through reactions with OH and NO_3.[66] Thus, the $NO_2 + HI$ reaction cannot be a major source of nitrous acid production in the troposphere.

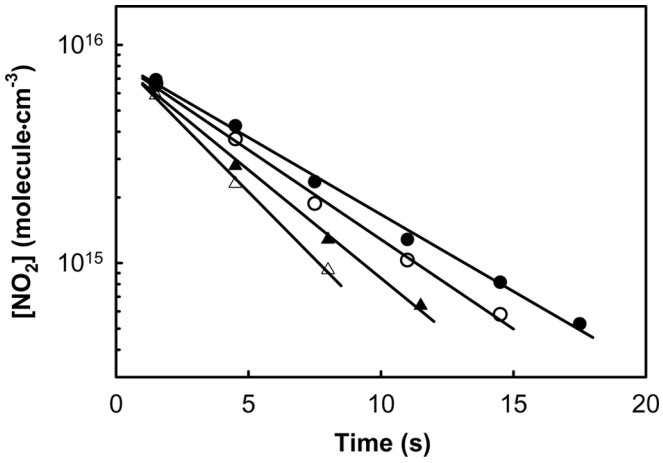

FIGURE 10 **Plot of log $[NO_2]$ versus reaction time t for the reaction of $NO_2 + HI$ at 303 K. The initial concentration of HI was: (•) 5.4×10^{16}, (o) 7.9×10^{16}, (▲) 1.0×10^{17}, (△) 1.3×10^{17} molecule·cm^{-3}, while $[NO_2]_0 = 6.8 \times 10^{15}$ molecule·cm^{-3}. The pseudo first-order rate constant k_{1st} was determined to be 0.16, 0.19, 0.23, and 0.28 s^{-1}, respectively. k_{1st} increased as the [HI] increased. (Adapted from [64] with permission the PCCP Owner Societies.).**

SUMMARY

In this paper, the application of QMS and FTIR to the study of chemical reactions at atmospherically relevant conditions was reviewed. A combination of coated-wall flow reactor with differentially pumped QMS is a very powerful analytical methodology to study chemical kinetics (both gas-phase and heterogeneous kinetics). The RAIRS-TPD technique allows the obtaining structural information of the adsorbed complex and the desorbed products simultaneously. The spectroscopic methods used in these studies are suited not only to atmospheric chemistry studies but also to surface chemistry studies and studies of chemical kinetics. The results obtained from these studies have advanced/provided in the understanding of the S(IV) oxidation by either HOBr or HOCl in the boundary layer, structural information on the molecularly adsorbed oxalic acid multilayer and assessed the roles of NO_2 and HI in atmosphere.

Currently, these spectroscopic techniques are being applied to study the adsorption of both oxalic acid/H_2O and H_2O/oxalic acid on Cu[67] and also to study the uptake of polyaromatic hydrogen carbons on single-walled carbon nanotubes.

ACKNOWLEDGMENT

This work was supported by the National Science Foundation (grant ATM-0355521).

REFERENCES

1. Solomon, S.; Garcia, R. R.; Rowland, F. S.; Wuebbles, D. J. On the depletion of Antarctic ozone. *Nature* **1986**, *321*, 755–758.
2. Solomon, S. Stratospheric ozone depletion: A review of concepts and history. *Rev. Geophys.* **1999**, *37*, 275–316.
3. Molina, M. J.; Tso, T. L.; Molina, L. T.; Wang, F. C. Y. Antarctic stratospheric chemistry of chlorine nitrate, hydrogen chloride, and ice: Release of active chlorine. *Science* **1987**, *238*, 1253–1257.
4. Tolbert, M. A.; Rossi, M. J.; Malhotra, R.; Golden, D. M. Reaction of chlorine nitrate with hydrogen chloride and water at Antarctic stratospheric temperatures. *Science* **1987**, *238*, 1258–1260.
5. Zondlo, M. A.; Hudson, P. K.; Prenni, A. J.; Tolbert, M. A. Chemistry and microphysics of polar stratospheric clouds and cirrus clouds. *Annu. Rev. Phys. Chem.* **2000**, *51*, 473–499.
6. Barrie, L. A.; Bottenheim, J. W.; Schnell, R. C.; Crutzen, P. J.; Rasmussen, R. A. Ozone destruction and photochemical reactions at polar sunrise in the lower Arctic atomosphere. *Nature* **1988**, *334*, 138–141.
7. Platt, U.; Hönninger, G. The role of halogen species in the troposphere. *Chemosphere* **2003**, *52*, 325–338.
8. Fan, S. M.; Jacob, D. J. Surface ozone depletion in Arctic spring sustained by bromine reactions on aerosols. *Nature* **1992**, *359*, 522–524.
9. Foster, K. L.; Plastridge, R. A.; Bottenheim, J. W.; Shepson, P. B.; Finlayson-Pitts, B. J.; Spicer, C. W. The role of Br_2 and BrCl in surface ozone destruction at polar sunrise. *Science* **2001**, *291*, 471–474.
10. McConnell, J. C.; Henderson, G. S.; Barrie, L.; Bottenheim, J.; Niki, H.; Langford, C. H.; Templeton, E. M. J. Photochemical bromine production implicated in Arctic boundary-layer ozone depletion. *Nature* **1992**, *355*, 150–152.
11. Finlayson-Pitts, B. J.; Pitts, Jr., J. N. *Chemistry of the Upper and Lower Atmosphere*; Academic: San Diego, 2000; Chapters 8 and 9.
12. Niki, H. In *Progress and Problems in Atmospheric Chemistry*; Barker, J. R., Ed.; World Scientific: Singapore, 1995; Chapter 3: Depletion of tropospheric ozone during Artic spring: Field and laboratory studies of the role of hydrocarbons.
13. Vogt, R.; Crutzen, P. J.; Sander, R. A mechanism for halogen release from sea-salt aerosol in the remote marine boundary layer. *Nature* **1996**, *383*, 327–330.
14. Narukawa, M.; Kawamura, K.; Li, S.-M.; Bottenheim, J. W. Dicarboxylic acids in the Arctic aerosols and snowpacks collected during ALERT 2000. *Atmos. Environ.* **2002**, *36*, 2491–2499.
15. Seinfeld, J. N.; Pandis, S. N. *Atmospheric Chemistry and Physics*; Wiley: New York, 1998; Chapters 5 and 6.
16. Saxena, P.; Hildemann, L. M. Water-soluble organics in atmospheric particles: A critical review of the literature and application of thermodynamics to identify candidate compounds. *J. Atmos. Chem.* **1996**, *24*, 57–109.
17. Kubicki, J. D.; Schroeter, L. M.; Itoh, M. J.; Nguyen, B. N.; Apitz, S. E. Attenuated total reflectance Fourier-transform infrared spectroscopy of carboxylic acids adsorbed onto mineral surfaces. *Geochim. Cosmochim. Acta* **1999**, *63*, 2709–2725.
18. Chu, L. T.; Leu, M.-T.; Keyser, L. F. Uptake of HCl in water–ice and nitric acid ice films. *J. Phys. Chem.* **1993**, *97*, 7779–7785.
19. Koch, T. G.; Rossi, M. J. Direct measurement of surface residence times: Nitryl chloride and chlorine nitrate on alkali halides at room temperature. *J. Phys. Chem. A* **1998**, *102*, 9193–9201.
20. Golden, D. M.; Spokes, G. N.; Benson, S. W. Very low-pressure pyrolysis (VLPP); a versatile kinetic tool. *Angew. Chem., Int. Ed. Engl.* **1973**, *12*, 534–546.
21. Quinlan, M. A.; Reihs, C. M.; Golden, D. M.; Tolbert, M. A. Heterogeneous reactions on model polar stratospheric cloud surfaces: reaction of N_2O_5 on ice and nitric acid trihydrate. *J. Phys. Chem.* **1990**, *94*, 3255–3260.
22. Hoffman, R. C.; Gebel, M. E.; Fox, B. S.; Finlayson-Pitts, B. J. Knudsen cell studies of the reactions of N_2O_5 and $ClONO_2$ with NaCl: Development and application of a model for estimating available surface areas and corrected uptake coefficients. *Phys. Chem. Chem. Phys.* **2003**, *5*, 1780–1789.
23. Finlayson-Pitts, B. J.; Wingen, L. M.; Sumner, A. L.; Syomin, D.; Ramazan, K. A. The heterogeneous hydrolysis of NO_2 in laboratory systems and in outdoor and indoor atmospheres: An integrated mechanism. *Phys. Chem. Chem. Phys.* **2003**, *5*, 223–242.
24. Nathanson, G. M.; Davidovits, P.; Worsnop, D. R.; Kolb, C. E. Dynamics and kinetics at the gas-liquid interface. *J. Phys. Chem.* **1996**, *100*, 13007–13020.
25. Behnke, W.; George, C.; Scheer, V.; Zetzsch, C. Production and decay of $ClNO_2$ from the reaction of gaseous N_2O_5 with NaCl solution: Bulk and aerosol experiments. *J. Geophys. Res.* **1997**, *102*, 3795–3804.
26. Zhang, X.; Zhuang, G.; Chen, J.; Wang, Y.; Wang, X.; An, Z.; Zhang, P. Heterogeneous reactions of sulfur dioxide on typical mineral particles. *J. Phys. Chem. B* **2006**, *110*, 12588–12596.
27. Wiesen, P.; Kleffmann, J.; Kurtenbach, R.; Becker, K. H. Mechanistic study of the heterogeneous conversion of NO_2 into HONO and N_2O on acid surfaces. *Faraday Discuss.* **1995**, *100*, 121–127.
28. Greenler, R. G. Infrared study of adsorbed molecules on metal surfaces by reflection techniques. *J. Chem. Phys.* **1966**, *44*, 310–315.
29. Greenler, R. G. Reflection method for obtaining the infrared spectrum of a thin layer on a metal surface. *J. Chem. Phys.* **1969**, *50*, 1963–1968.

30. Bolina, A. S.; Wolff, A. J.; Brown, W. A. Reflection absorption infrared spectroscopy and temperature-programmed desorption studies of the adsorption and desorption of amorphous and crystalline water on a graphite surface. *J. Phys. Chem. B* **2005**, *109*, 16836–16845.
31. Barros, R. B.; Garcia, A. R.; Ilharco, L. M. The chemistry of formic acid on oxygen modified Ru(001) surfaces. *Surf. Sci.* **2005**, *591*, 142–152.
32. Banham, S. F.; Sodeau, J. R.; Horn, A. B.; McCoustra, M. R. S.; Chesters, M. A. Adsorption and ionization of HCl on an ice surface. *J. Vac. Sci. Technol. A* **1996**, *14*, 1620–1626.
33. Chu, L. T.; Heron, J. W. Uptake of HBr on ice at polar atmospheric conditions. *Geophys. Res. Lett.* **1995**, *22*, 3211–3214.
34. Chu, L.; Chu, L. T. Heterogeneous reaction $HOCl + HBr \rightarrow BrCl + H_2O$ on ice films. *J. Phys. Chem. A* **1999**, *103*, 691–699.
35. Chu, L. T. Safety interlock and remote computer monitoring for a diffusion-pumped vacuum system. *J. Vac. Sci. Technol. A* **1997**, *15*, 201–205.
36. NIST. *Chemistry webbook*. Available at http://webbook.nist.gov/chemistry/
37. Keyser, L. F.; Leu, M.-T. Surface areas and porosities of ices used to simulate stratospheric clouds. *J. Colloid Interface Sci.* **1993**, *155*, 137–145.
38. Jin, R.; Chu, L. T. Uptake of SO_2 on HOBr-ice surfaces. *J. Phys. Chem. A* **2006**, *110*, 3647–3654.
39. Chu, L.; Chu, L. T. Heterogeneous interaction and reaction of HOBr on ice films. *J. Phys. Chem. A* **1999**, *103*, 8640–8649.
40. Jin, R.; Chu, L. T. Heterogeneous reactions of SO_2 with HOCl and HOBr on ice surfaces. *J. Phys. Chem. A* **2006**, *110*, 8719–8728.
41. Keene, W. C.; Sander, R.; Pszenny, A. A. P.; Vogt, R.; Crutzen, P. J.; Galloway, J. N. Aerosol pH in the marine boundary layer: A review and model evaluation. *J. Aerosol Sci.* **1998**, *29*, 339–356.
42. Fogelman, K. D.; Walker, D. M.; Margerum, D. W. Non-metal redox kinetics: Hypochlorite and hypochlorous acid reactions with sulfite. *Inorg. Chem.* **1989**, *28*, 986–993.
43. Hartz, K. E. H.; Nicoson, J. S.; Wang, L.; Margerum, D. W. Kinetics and mechanisms of S(IV) reduction of bromite and chlorite ions. *Inorg. Chem.* **2003**, *42*, 78–87.
44. Troy, R. C.; Margerum, D. W. Non-metal redox kinetics: Hypobromite and hypobromous acid reactions with iodide and with sulfite and the hydrolysis of bromosulfate. *Inorg. Chem.* **1991**, *30*, 3538–3543.
45. Brown, R. L. Tubular flow reactors with first-order kinetics. *J. Res. Natl. Bur. Stand. (U.S.)* **1978**, *83*, 1–8.
46. Chu, L.; Diao, G. W.; Chu, L. T. Heterogeneous interaction of SO_2 on H_2O_2-ice films at 190–210 K. *J. Phys. Chem. A* **2000**, *104*, 7565–7573.
47. Cussler, E. L. *Diffusion, Mass Transfer in Fluid Systems*; Cambridge University: New York, 1984; Chapter 4.
48. Chu, L. T.; Leu, M.-T.; Keyser, L. F. Heterogeneous reactions of $HOCl + HCl \rightarrow Cl_2 + H_2O$ and $ClONO_2 + HCl \rightarrow Cl_2 + HNO_3$ on ice surfaces at polar stratospheric conditions. *J. Phys. Chem.* **1993**, *97*, 12798–12804.
49. Chu, L.; Chu, L. T. Heterogeneous bromine interactions on ice surfaces at the atmospheric temperature. *Recent Res. Devel. Geophysics* **2000**, *3*, 141–151.
50. Keyser, L. F.; Moore, S. B.; Leu, M.-T. Surface reaction and pore diffusion in flow-tube reactors. *J. Phys. Chem.* **1991**, *95*, 5496–5502.
51. Keyser, L. F.; Leu, M.-T. Morphology of nitric acid and water ice films. *Microsc. Res. Tech.* **1993**, *25*, 434–438.
52. Keyser, L. F.; Leu, M.-T.; Moore, S. B. Comment on porosities of ice films used to simulate stratospheric cloud surfaces. *J. Phys. Chem.* **1993**, *97*, 2800–2801.
53. Hug, S. J.; Sulzberger, B. *In situ* Fourier transform infrared spectroscopic evidence for the formation of several different surface complexes of oxalate on TiO_2 in the aqueous phase. *Langmuir* **1994**, *10*, 3587–3597.
54. Martin, D. S.; Cole, R. J.; Haq, S. Investigating the adsorption of oxalic acid onto Cu(110) to create a chemically functionalised surface. *Surf. Sci.* **2003**, *539*, 171–181.
55. Bellamy, L. J.; Pace, R. J. Hydrogen bonding in carboxylic acids-I. oxalic acids. *Spectrochim. Acta* **1963**, *19*, 435–442.
56. de Villepin, J.; Novak, A. Spectres de vibration des acides oxaliques. I. Spectres infrarouge et raman de la phase β des acides $H_2C_2O_4$, $D_2C_2O_4$, $H_2C_2{}^{18}O_4$ et $D_2C_2{}^{18}O_4$. *Spectrochim. Acta, Part A* **1978**, *34*, 1009–1017.
57. de Villepin, J.; Novak, A.; Dougeard, D. α- and β-phases of oxalic acid, $H_2C_2O_4$: Vibrational spectra, normal-coordinate calculations, and intermolecular forces. *Chem. Phys.* **1982**, *73*, 291–312.
58. Hellebust, S.; O'Riordan, Sodeau, J. Cirrus cloud mimics in the laboratory: An infrared spectroscopy study of thin films of mixed ice of water with organic acids and ammonia. *J. Chem. Phys.* **2007**, *126*, 084702.
59. Weisel, M. D.; Chen, J. G.; Hoffmann, F. M.; Sun, Y.-K.; Weinberg, W. H. A Fourier transform-infrared reflection absorption spectroscopy study of the formation and decomposition of chemisorbed formate on clean and potassium-modified Ru(001). *J. Chem. Phys.* **1992**, *97*, 9396–9411.
60. Chu, L. T.; Chu, L. Uptake and interaction of HI on ice films. *J. Phys. Chem. B* **1997**, *101*, 6271–6275.
61. Diao, G. W.; Chu, L. T. Heterogeneous reactions of $HX + HONO$ and I_2 on ice surfaces: Kinetics and linear correlations. *J. Phys. Chem. A* **2005**, *109*, 1364–1373.
62. Calvert, J. G.; Yardwood, G.; Dunker, A. M. An evaluation of the mechanism of nitrous acid formation in the urban atmosphere. *Res. Chem. Intermed.* **1994**, *20*, 463–502.
63. Rosser, Jr., W. A.; Wise, H. Kinetics of the gas phase oxidation of hydrogen chloride and of hydrogen bromide by nitrogen dioxide. *J. Phys. Chem.* **1960**, *64*, 602–604.
64. Diao, G.; Chu, L. T. A kinetic study of the reaction of NO_2 with HI over the temperature range 278 to 333 K. *Phys. Chem. Chem. Phys.* **2001**, *3*, 1622–1630.
65. Barney, W. S.; Wingen, L. M.; Lakin, M. J.; Brauers, T.; Stutz, J.; Finlayson-Pitts, B. J. Infrared absorption cross-section measurements for nitrous acid (HONO) at room temperature. *J. Phys. Chem. A* **2000**, *104*, 1692–1699.
66. Vogt, R.; Sander, R.; Von Glasow, R.; Crutzen, P. J. Iodine chemistry and its role in halogen activation and ozone loss in the marine boundary layer: A model study. *J. Atmos. Chem.* **1999**, *32*, 375–395.
67. Yan, H.; Chu, L. T. Interaction of oxalic acid and ice on Cu surface. *Langmuir* **2008**, *24*, 9410–9420.